Article

Not peer-reviewed version

Antiproliferative And Ultrastructural Analysis Triggered by Drugs Contained In The Medicines for Malaria Venture Covid-Box Against Toxoplasma gondii Tachyzoites

Andreia Luiza Oliveira Costa , Mike dos Santos , Rosalida Estevam Nazar Lopes , Rossiane C. Vommaro , Érica S. Martins-Duarte *

Posted Date: 14 August 2024

doi: 10.20944/preprints202408.1034.v1

Keywords: Toxoplasmosis; Drug Repositioning; Apicomplexa; Cycloheximide; Bortezomib

 doi:10.20944/preprints202408.1034.v1

Article

Antiproliferative And Ultrastructural Analysis Triggered by Drugs Contained In The Medicines for Malaria Venture Covid-Box Against *Toxoplasma gondii* Tachyzoites

Andréia Luiza Oliveira Costa [1], Mike dos Santos [1], Rosálida Estevam Nazar Lopes [1], Rossiane Claudia Vommaro [2] and Érica S. Martins-Duarte [1,*]

[1] Laboratório de Quimioterapia de Protozoários Egler Chiari, Departamento de Parasitologia - ICB, Universidade Federal de Minas Gerais, Belo Horizonte, MG, 31270-901, Brazil;
[2] Laboratório de Ultraestrutura Celular Hertha Meyer, Instituto de Biofísica Carlos Chagas Filho, Centro de Pesquisa em Medicina de Precisão, Universidade Federal do Rio de Janeiro, Rio de Janeiro, RJ, Brazil;
* Correspondence: ericamduarte@icb.ufmg.br; Tel.: +55 (31) 3409.2847

Abstract: *Toxoplasma gondii* is a protozoan and the etiologic agent of toxoplasmosis causes high mortality in immunocompromised individuals and newborns. Despite the medical importance of toxoplasmosis; few drugs are available for its treatment; which are associated with side events and parasite resistance. Here; we show a screening of molecules present in Covid-Box as a way of discovering new hits with anti-*T. gondii* activity. Covid-Box contains 160 molecules with known or predicted activity against SARS-CoV-2. Our analysis selected 23 Covid-Box molecules that can inhibit the tachyzoite forms of the RH strain of *T. gondii* in vitro by more than 70% at 1 μM after seven days of treatment. The inhibitory curves showed that most of these molecules inhibited the proliferation of tachyzoites with IC_{50} values below 0.80 μM; Cycloheximide and (-)-Anisomycin were the most active drugs; with IC_{50} values of 0.02 μM. Cell viability assays showed that the compounds are not toxic at active concentrations; and most are highly selective for parasites. Overall; all 23 compounds were selective; and for three of them (Apilimod; Midostaurin; and Salinomycin); this is the first report of activity against *T. gondii*. To better understand the effect of the drugs; we analyzed the effect of six of them on the ultrastructure of *T. gondii* using transmission electron microscopy. The main changes observed in parasite morphology after treatment with the selected drugs were changes in cell division and parasite organelles

Keywords: toxoplasmosis; drug repositioning; apicomplexa; cycloheximide; bortezomib

1. Introduction

Toxoplasma gondii is the etiologic agent of toxoplasmosis, a zoonosis with a high proportion of seropositive individuals worldwide [1]. The importance of this disease for humans is related to the high morbidity of immunocompromised individuals, such as AIDS patients and newborns [2]. *T. gondii* infection is asymptomatic in 80% of infected individuals. However, primary infection in AIDS patients can cause the cerebral form of the disease [3].

Congenitally infected newborns can develop neurological problems and eye diseases [4]. In Europe, a risk of eye damage cases of 0.3% to 1% has been observed in adults one or two years after acquiring the infection, and retinochoroiditis results in higher damage in America than in Europe or North America [5,6]. It is believed that 400 to 4.000 children are born with toxoplasmosis each year in the United States [7]. In Brazil, the incidence of congenital transmission can reach 1:770 live births [4], and the estimated prevalence of toxoplasmosis is 42 to 92%, depending on the region of the country [8].

Despite the medical importance of toxoplasmosis, few drugs are available for their treatment [9]. The combination of pyrimethamine (PYR), sulfadiazine (SDZ), and folinic acid has been administered for approximately 70 years. This association is still the first choice for all clinical conditions of the

 doi:10.20944/preprints202408.1034.v1

disease [10]. However, this therapeutic scheme has some critical flaws, such as frequent and non-tolerated side effects, which lead to the abandonment of treatment. In addition, there are reports of therapeutic failures with T. gondii strains possibly resistant to these drugs, as well as low absorption and the need for high therapeutic doses or a long-period treatment, making it challenging to manage the treatment [11–13].

In this context, drug repositioning has been a promising strategy for new treatments for infectious and neglected diseases. This strategy consists of redirecting an active pharmaceutical compound with commercial use or in development and reusing it for a new therapeutic indication. The development and discovery of medicines are a long and high-investment process [14,15]. Based on this, the Medicines for Malaria Venture (MMV) develops and offers several promising drug libraries with potential repositioning for treating neglected diseases and infections that can cause epidemics. The first drug box provided by MMV was in 2014, Malaria-Box. The anti-*T. gondii* activity of the compounds available in Malaria-Box has already been described in the literature [16–18]. Several other compounds present in other boxes such as, Pathogen Box and Pandemic Box, have also shown anti-*T. gondii* activity [19–22].

In 2020, with the advent of the COVID-19 pandemic, MMV made available a new box with 160 drugs and compounds, Covid-Box. The drugs and compounds in this box have structurally different therapeutic classes, selected by experts and initially tested against the new coronavirus (SARS-COV-2). As Covid-Box compounds are in various stages of pharmacological research and development and considering the need to identify new potential treatments for toxoplasmosis and the potential of Covid-Box, this work aimed to expand the study of the activity of these compounds against the tachyzoites of *T. gondii* and characterize the effect of the best ones on the ultrastructure of the parasite.

2. Materials and Methods

2.1. Drugs and Compounds of Covid-Box

The 160 drugs and compounds were provided free of charge by MMV (https://www.mmv.org/mmv-open/covid-box/covid-box-supporting-information), where the compounds were physically made available as 10 mM solubilized solutions in DMSO in two 96-well plates (A and B) containing 80 compounds each. For storage in this box, the drugs and compounds were dissolved in reserves of 2 mM with 100% DMSO (Merck).

2.2. Parasites

T. gondii tachyzoites of the RH strain were used. Parasite was maintained in vitro through serial passages in 25 cm2 culture flasks of confluent neonatal Normal Human Dermal Fibroblastic Cells (NHDF; Lonza, kindly donated by Dr. Sheila Nardelli, Fiocruz Paraná) in RPMI 1640 medium supplemented with 2% Fetal Bovine Serum (Gibco), Penicillin/Streptomycin, Amphotericin B (Life Technologies, Eugene, OR, USA), and 2 mM glutamine (complete medium). Cells and parasites were maintained at 37°C in a humid atmosphere of 5% CO_2.

2.3. Antiproliferative Assays against Tachyzoite Stage

For preliminary evaluation of the 160 drugs and compounds in the Covid-Box, 6-well plates with monolayers of NHDF cells in complete RPMI-1640 medium were infected with 1.000 newly egressed tachyzoites of *T. gondii* and treated with 1 μM of each drug. For antiproliferative curves, 12-well plates were used, and cells were infected with 600 tachyzoites. After the addition of the parasites, decreasing concentrations of drugs and compounds (1 μM – 0.0078 μM in two-fold serial dilutions) were added to each well. In the control wells, 0.1% DMSO was added. After 7 days of treatment, the cells were fixed with 70% ethanol and stained with crystal violet. Stained plates were imaged with ChemiDoc MP Imaging System (Bio-Rad), and then plaque areas were analyzed with the ImageJ® software (version 1.52e). Total destruction areas of treated cells were quantified and compared with the untreated (control) to determine the percentage of proliferation and inhibition of T. gondii. For the calculation of the inhibitory concentration of 50% (IC_{50}), the growth inhibition percentage was plotted

 doi:10.20944/preprints202408.1034.v1

as a function of drug concentration by fitting the values to the standard curve analysis. The regression analyses were performed using GraphPad Prism 8 Software (GraphPad Inc., San Diego, CA, USA).

2.4. Cytotoxicity Assay in NHDF Cell

The cytotoxic effect of Covid-Box drugs and compounds against NHDF cells was evaluated by the MTS assay [25,26]. For this, 96-well tissue plates containing NHDF cells were treated with different concentrations of drugs and compounds for seven days. At the end of the treatment, the cells were washed with PBS, each well was filled with 100 µL of 10 mM Glucose in PBS and 20 µL of MTS reagent (Promega, Madison, WI, USA) was added. The absorbance was read at 490 nm after 3 h of incubation at 37°C. Cytotoxicity was calculated as the percentage of viable cells versus untreated cells (control). The Cytotoxic Concentration of 50% (CC_{50}) for the host cells was calculated as for IC_{50}, and the Selective Index (SI) was calculated as the ratio of CC_{50}/IC_{50}.

2.5. Druggability Analysis of Drugs and Compounds

For the *in silico* analysis, the chemical structures of the simplified molecular line input system (SMILES) code from all drugs were obtained from the plate map available at https://www.mmv.org/mmv-open/covid-box/covid-box-supporting-information and loaded into the online programs pkCSM (https://biosig.lab.uq.edu.au/pkcsm/prediction) and SwissADME (http://www.swissadme.ch/) for physicochemical, toxicity and pharmacokinetics properties analysis of the drugs and compounds of Covid-Box. Pyrimethamine (PYR), Sulfadiazine (SDZ), Clindamycin (CLI), Azithromycin (AZT), and Atovaquone (ATO) were analyzed as reference drugs.

2.6 Transmission Electron Microscopy (TEM)

NHDF cultures infected with T. gondii were treated with compounds and fixed with 2.5% glutaraldehyde in 0.1 M sodium cacodylate buffer (pH 7.4). Cells were post-fixed for with 1% osmium tetroxide, 1.25% potassium ferrocyanide, and 5 mM $CaCl_2$, in 0.1 M sodium cacodylate buffer (pH 7.4). The sample fixation and processing for microscopy were performed as previously described [27]. Samples were dehydrated in alcohol solutions of increasing concentrations (35–100%) and embedded in Epoxy resin (Polybed 812). Ultrathin sections were collected in copper grids, stained with uranyl acetate and lead citrate, and then observed in a Fei TecNai G2 120 kV Spirit Electron Microscope.

2.7. Statistical Analysis

Data were analyzed using GraphPad Prism 8.0 software (GraphPad Inc., San Diego, CA, USA). IC_{50} and CC_{50} calculations were done by fitting the values of proliferation/ viability in percentage to a non-linear curve followed by dose-response inhibition analysis through log(inhibitor) vs. normalized response.

3. Results

3.1. Drugs of Covid-Box Showed High Activity and Selectivity against T. gondii Tachyzoites

The antiproliferative effect of 1µM of each 160 drugs and compounds present in the Covid-Box was screened against tachyzoites of the RH strain of *T. gondii* for seven days of treatment. Thirty compounds inhibited parasite proliferation in at least 70% (Figure 1A-H). Of the 30 best drugs, seven were excluded from the studies. Two (AF03, Amiodarone - MMV001992; BC06, Proscillaridin - MMV001433) were initially excluded because they presented signs of cytotoxicity for the host cells during the initial screening. Other five drugs (Itraconazole (AC06 - MMV637528); Doxycycline (AE05 - MMV000011); Cyclosporine (AF04 - MMV001860); Doxorubicin (BA05 - MMV004066); Digitoxin (BC04 - MMV002436) were excluded as their activity *T. gondii* have been extensively studied before [23,28–33] (See details of the compounds and drugs in https://www.mmv.org/mmv-open/covid-box/covid-box-supporting-information). Thus, 23 drugs were selected for the IC_{50} and cytotoxicity analysis (Table 1).

 doi:10.20944/preprints202408.1034.v1

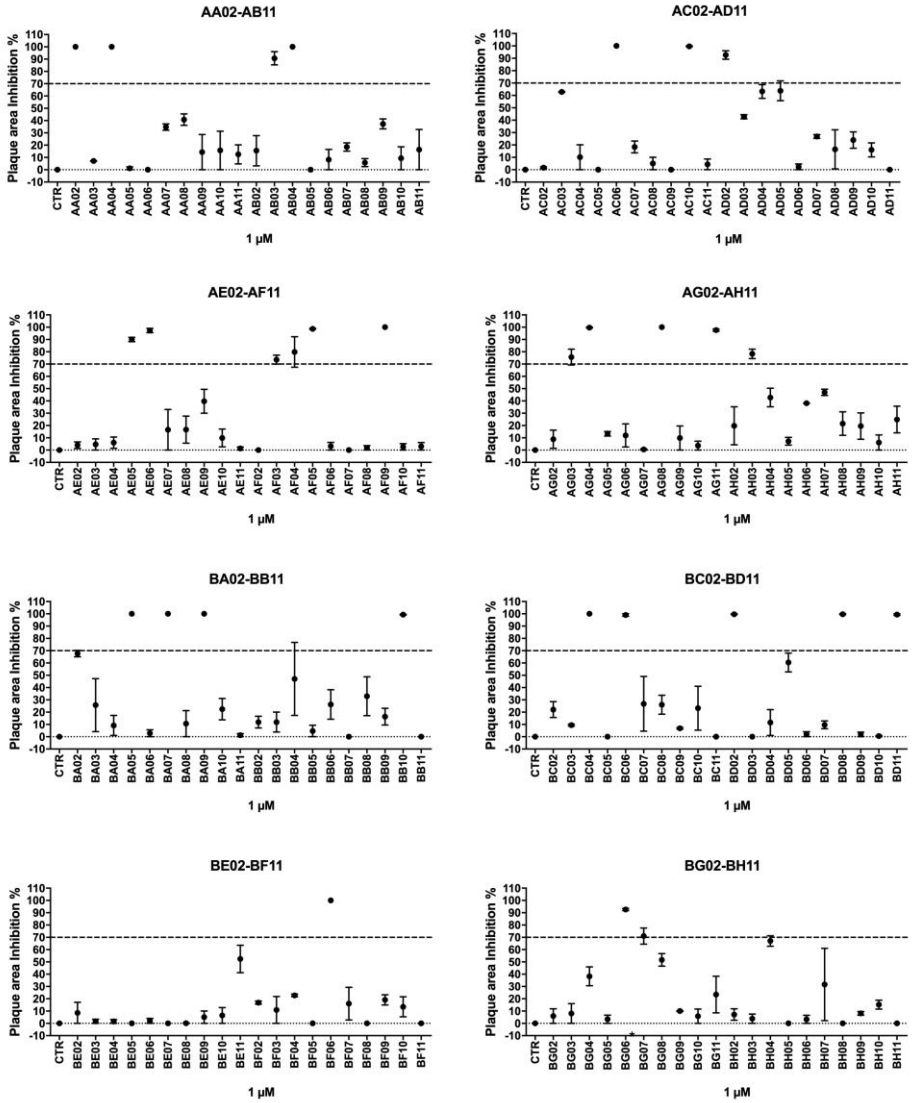

Figure 1. A-H. Preliminary evaluation of the effectiveness of 160 drugs and compounds from Covid-Box against *T. gondii* tachyzoites. After obtaining the NDHF cell monolayer, the cells were infected with 600 RH strain tachyzoites. After infection, each well of the plate was treated at a concentration of 1µM of each drug. Values represent mean ± SD of two experiments. CTR= Control.

Table 1. IC_{50} values and cytotoxicity of drugs and compounds of Covid-Box.

Plate Position	MMV ID	Trivial Name	Disease Area	Status[a]	IC_{50} (µM) in tachyzoites of RH strain	Cytotoxicity against NHDF		Anti-*T. gondii* activity[c]
						CC_{50} (µM)	SI[b]	
AA02	**MMV003461**	**Niclosamide**	**Antiparasitic**	**Approved**	**0.36 ± 0.02**	3.05 ± 0.08	8	Yes [24,34]
AA04	MMV1804190	Bemcentinib	Immune agent	Phase II	0.15 ± 0.03	0.97 ± 0.15	6	Yes [24]
AB03	MMV1804187	Apilimode	Antitumor agent	Phase II	0.22 ± 0.06	2.12 ± 0.12	10	New
AB04	MMV1804185	Regorafenibe	Antitumor Agent	Approved	0.25 ± 0.04	3.03 ± 0.01	12	Yes [24]
AC10	MMV690777	LY2228820	Antitumor agent	Phase II, discontinued	0.04 ± 0.00	nd	nd	Yes [24]
AD02	MMV002832	Digoxin	Antiarrhythmic	Approved	0.03 ± 0.01	0.34 ± 0.32	11	Yes [23]
AE06	MMV688731	Emetine	Antiparasitic	Approved	0.05 ± 0.01	1.02 ± 0.19	20	Yes [35]
AF05	MMV672931	Ivermectin	Antiparasitic	Approved	0.21 ± 0.01	nd	nd	Yes [36]
AF09	MMV010306	Sorafenib	Antitumor agent	Approved	0.56 ± 0.03	nd	nd	Yes [24]
AG03	MMV1804194	Manidipine	Antihypertensive	Phase III	0.74 ± 0.09	nd	nd	Yes [24]
AG04	MMV1804175	Almitrine	Respiratory systemAgent	Approved*	0.33 ± 0.04	nd	n.d	Yes [23,24]
AG08	MMV010288	Midostaurin	Antitumor agent	Approved	0.08 ± 0.00	0.24 ± 0.02	3	New

 doi:10.20944/preprints202408.1034.v1

AG11	MMV1804174	Abemaciclib	Antitumor agent	Approved	0.09 ± 0.01	#	#	Yes [24]
AH03	MMV003277	Tetrandrine	Antitumor Agent	Preclinical	0.35 ± 0.07	4.77 ± 8.25	14	Yes [24]
BA07	MMV1580167	Ponatinib	Antitumor agent	Approved	0.33 ± 0.03	4.84 ± 0.89	15	Yes [33]
BA09	MMV007474	Berbamine	Antitumor Agent	Preclinical	0.31 ± 0.03	4.61 ± 7.52	15	Yes [24]
BB10	MMV003219	Mycophenolic acid	Immunosuppressant	Approved	0.07 ± 0.01	23.81 ± 31.97	340	Yes [37,38]
BD02	MMV1804312	Salinomycin	Anti-microbial agent	Approved	0.07 ± 0.01	1.14 ± 0.17	16	New
BD08	MMV1804359	Merimepodib	Antiviral agent	Phase II	0.48 ± 0.08	nd	nd	Yes [24]
BD11	MMV000031	Cycloheximide	Agricultural agent – Fungicid	Research	0.02 ± 0.00	6.08 ± 4.63	304	Yes [39,40]
BF06	MMV1634116	(-) -Anisomycin	Anti-infective agent	Approved	0.02 ± 0.00	0.25 ± 0.13	13	Yes [41]
BG06	MMV009415	Bortezomib	Antitumor agent	Approved	0.03 ± 0.00	0.72 ± 0.24	24	Yes [23,33]
BG07	MMV002137	Pimozide	Antipsychotic	Approved	0.64 ± 0.15	nd	nd	Yes [23,32]

nd = not determined. Concentrations up to 3 μM did not affect NHDF cells proliferation. #There was not enough to perform this assay.[a]Approved: FDA-approved marketed drug; Phase III: Clinical candidate drug in Phase 3 clinical trials; Phase II: Clinical candidate drug in Phase 2 clinical trials; Phase I: Clinical candidate drug in Phase 1 clinical trials; *Almitrine was withdrawn in some countries. [b] Selectivity Index, calculated based on the CC_{50} NDHF cells/IC_{50} *T. gondii* ratio after 7 days of treatment. [c] We searched on PubMed the trivial name of each compound plus "*Toxoplasma gondii*". If available, the reference for a previous study was included. The term "New" indicates when no results were retrieved from the search.

The drugs Cycloheximide (MMV000031), Bortezomib (MMV009415), Digoxin (MMV002832), and (-) -Anisomycin (MMV1634116) were the most active, inhibiting the proliferation of *T. gondii* with IC_{50}s values lower than or equal to 30 nM (Table 1). The drugs Salinomycin, Mycophenolic acid, Abemaciclib, Midostaurin, Emetine, and LY2228820 inhibited T. gondii proliferation with IC_{50} lower than 100 nM (Table 1). The drugs Ivermectin (MMV672931), Almitrine (MMV1804175), Apilimode (MMV1804187), Bemcentinib (MMV1804190), Niclosamide (MMV003461), Regorafenibe (MMV1804185), and Merimepodib (MMV1804359) were also highly active against *T. gondii*, presenting IC_{50} in the range of 0.15 – 0.48 μM (Table 1).

The cytotoxicity assay showed that most compounds were highly selective against *T. gondii*, and the SI ranged from 3 to 304 (Table 1). Drugs with IC_{50}s less than 30 nM (Cycloheximide and Bortezomib) had the highest SI. Overall, all 23 compounds were selective, and for three of them (Apilimod, Midostaurin, and Salinomycin), this is the first report of activity against *T. gondii* (Table 1).

3.2. Covid-Box Drugs Show Potential Oral Druggability

Through the SwissADME [42] platform it was possible to obtain information about the physical-chemical properties of the drugs that showed the best activity against *T. gondii*. From these analyses, it was possible to predict whether these compounds are in accordance with the predictors of Lipinski's rule of 5 (RO5) and Veber (Table 2). We also compared PYR, SDZ, CLI, AZT, and ATO, which are currently used for treating toxoplasmosis. RO5 states that drugs with more than 5H-bond donors, more than 10H-bond acceptors, molecular weight (MW) greater than 500, and calculated LogP (a measure of lipophilicity) greater than 5 are less likely to have good oral absorption and permeation. In addition to the RO5 of Lipinski et al. (1997) [43], the two predictors of Veber et al. (2002) [44] also point that compounds with Total Polar Surface Area (TPSA) equal to or < 140 Å2 and with ten or less rotating bonds have a greater chance of success in oral bioavailability.

The analyses were carried out for the 23 drugs from the Covid-Box selected in the antiproliferative assay and those used as the gold standard (PYR and SDZ) and alternative (AZT, CLI, and ATO) for toxoplasmosis. As expected, PYR and SDZ results agreed with Lipinski's RO5 and Veber's predictors. among the drugs used as alternative treatments, only AZT violates two Lipinski rules (MW and 5H-bond donors) and one Veber criterion (TPSA <140Å2) (Table 2). Of the 23 selected from the Covid-Box, 10 (AA02, AB03, AB04, AE06, AF09, BB10, BD08, BD11, BF06, and BG06) showed compliance with RO5 and Veber`s predictors (Table 2). The other drugs and compounds showed at least one or more non-compliance with RO5 and Veber (Table 2).

 doi:10.20944/preprints202408.1034.v1

Information on the pharmacokinetic properties of selected drugs from the Covid-Box and drugs already used in treating toxoplasmosis were obtained using the platform. Caco-2 permeability values (log Papp at 10-6 cm/s) above 0.90 predict high intestinal permeability. The drugs AA04, AB03, AC10, AG03, AG04, AG08, AG11, and BA07 had log Papp at 10-6 cm/s above 0.90, and AB04, AE06, AF09, AH03, and BB10 showed values of log Papp at 10-6cm/s > 0.70 – < 0.90, which can be inferred that these also have the potential to present high intestinal permeability [45]. The other drugs showed values below 0.60 log Papp at 10-6 cm/s (Table 3). It should also be noted that even the compound BD11, presenting a Caco-2 value below 0.90 (0.553 log Papp at 10-6 cm/s, Intestinal Absorption (Human) = 69.8 %) (Table 3) was the compound selected in the in vitro tests that most inhibited parasite proliferation with an IC_{50} value = 0.02 μM (Table 1). Volume of distribution values (VDSs) predict drug distribution in tissue. It is known that the lower the interaction of drugs with plasma proteins, the faster they will be absorbed and, therefore, the faster they will be directed to their site of action. Thus, the higher the VDSs value above 0.45 log L/kg, the more the drug is distributed in tissues than in plasma, and values below -0.15 L/kg are considered poorly distributed [45]. Seven drugs or compounds selected from the Covid-Box (AA04, AE06, AF05, AG03, AG04, AG11, and BA07 showed high distribution, and the drugs used for the treatment of toxoplasmosis: SDZ and 0.329), and Covid-Box: AA02, AC10, AD02, AF09, BD02, BD08, BD11, BF06, and BG07 showed VDss higher than -0.15 log L/kg (Table 3). Fraction unbound analyses showed that BF06 and BD11 were the drugs with higher proportion of free state in plasma (Table 3).

Table 2. Physical-chemical properties of drugs and compounds of Covid-Box according to RO5 predictors by Lipinski and Veber.

Identification		LogP[a]	H-bond donors	H-bond acceptors	MW[b]	n° violations Lipinski	TPSA (Å²)[c]	n° rotations	n° violations Veber
PYR	Pyrimethamine	2.84	2	4	248.72	0	77.83	2	0
SDZ	Sulfadiazine	0.86	3	5	250.28	0	98.57	3	0
CLI	Clindamycin	0.39	4	7	424.99	0	102.25	7	1
AZT	Azithromycin	2.50	5	14	749.00	2	198.54	7	1
ATO	Atovaquone	5.34	1	3	366.84	1	54.70	2	0
AA02	Niclosamide	3.85	2	4	327.12	0	128.62	3	0
AA04	Bemcentinib	4.88	2	8	506.66	2	92.35	4	0
AB03	Apilimode	3.08	1	8	418.50	0	84.77	8	0
AB04	Regorafenibe	4.39	3	7	482.82	0	92.35	5	0
AC10	LY2228820	5.51	2	5	420.54	1	85.41	5	0
AD02	Digoxin	2.22	6	14	780.95	3	203.06	7	1
AE06	Emetine	3.04	1	6	480.65	0	52.20	7	0
AF05	Ivermectin	4.37	3	14	875.11	2	170.06	8	1
AF09	Sorafenib	4.10	3	7	464.83	0	92.35	9	0
AG03	Manidipine	4.04	1	8	610.71	1	116.94	12	1
AG04	Almitrine	4.34	2	6	477.55	0	69.21	10	0
AG08	Midostaurin	4.05	1	4	570.65	1	77.73	4	0
AG11	Abemaciclib	4.04	1	8	506.59	1	75.00	7	0
AH03	Tetrandrine	5.49	0	8	622.75	2	61.86	4	0
BA07	Ponatinib	4.30	1	8	532.56	1	65.77	6	0
BA09	Berbamine	5.13	1	8	608.72	2	72.86	3	0
BB10	Mycophenolic acid	2.72	2	6	320.34	0	93.07	6	0
BD02	Salinomycin	4.98	4	11	751.01	2	161.21	12	2
BD08	Merimepodib	2.36	3	7	452.46	0	123.96	11	1
BD11	Cycloheximide	1.23	2	4	281.35	0	83.47	3	0
BF06	(-) -Anisomycin	1.00	2	5	265.30	0	67.79	5	0
BG06	Bortezomib	0.22	4	6	384.24	0	124.44	11	1
BG07	Pimozide	5.67	1	5	461.55	1	41.29	7	0

[a]LogP: octanol–water partition coefficient; [b]MW: molecular weight; TPSA: Total Polar Surface Area.

The Central Nervous System (CNS) is a common site of infection of *T. gondii*; thus, we evaluated the predictors for CNS and BBB permeability of the Covid-Box drugs (Table 3). For CNS permeability, compounds with logPS > -2 are predicted to penetrate, but with logPS < -3 are unable to penetrate.

 doi:10.20944/preprints202408.1034.v1

From the Covid-Box, six drugs (AA02, AC10, AF09, AG08, BA07, and BG07) showed a prediction of CNS penetration, and 12 presented logPS between -3 and -2 and had the potential for penetration, too (Table 3).

Table 3. Pharmacokinetic properties of drugs and compounds of Covid-Box according to pkCSM.

Identification		Caco-2 Permeability[a]	Intestinal Absorption (human)	Fraction Unbound (human)	VDss (Human)[b]	CNS permeability[c]	BBB permeability[d]
PYR	Pyrimethamine	0.927	92.74%	0.311	-0.307	-2.203	-0.166
SDZ	Sulfadiazine	0.702	73.92%	0.28	0.182	-2.87	-0.672
CLI	Clindamycin	0.063	53.28%	0.747	-0.206	-3.63	-0.943
AZT	Azithromycin	-0.211	45.81%	0.719	-0.214	-4.12	-1.494
ATO	Atovaquone	1.483	91.41%	0	0.329	-1.418	0.401
AA02	Niclosamide	0.886	89.48%	0	-0.022	-1.972	-0.626
AA04	Bemcentinib	1.654	91.04%	0.152	0.799	-2.097	-0,953
AB03	Apilimode	1.388	96.75%	0.044	-0.173	-2.901	-1.047
AB04	Regorafenibe	0.454	93.43%	0	-0.277	-2.031	-1.573
AC10	LY2228820	1.321	84.39%	0.367	0.066	-1.674	-1.378
AD02	Digoxin	0.381	78.23%	0.287	0.085	-4.19	-1.927
AE06	Emetine	1.333	95.40%	0.155	1.632	-2.041	0.045
AF05	Ivermectin	0.602	89.45%	0.126	0.587	-3.438	-2.000
AF09	Sorafenib	0.907	84.99%	0	-0.105	-1.995	-1.675
AG03	Manidipine	0.928	93.59%	0.086	0.683	-2.339	-0.998
AG04	Almitrine	1.392	87.59%	0.136	1.189	-2.727	-0.945
AG08	Midostaurin	0.985	98.28%	0.286	-1.663	-1.764	0.039
AG11	Abemaciclib	1.341	89.68%	0.097	0.614	-2.981	-1.665
AH03	Tetrandrine	0.737	92.83%	0.371	-0.808	-2.576	0.074
BA07	Ponatinib	1.000	91.44%	0.040	0.565	-1.862	0.278
BA09	Berbamine	1.143	92.79%	0.399	-0.999	-2.608	-0.936
BB10	Mycophenolic acid	0.244	62.24%	0.217	-0.651	-2.908	-0.159
BD02	Salinomycin	-0.140	58.65%	0.220	0.372	-3.068	-1.754
BD08	Merimepodib	1.024	93.76%	0	-0.122	-3.32	-1.647
BD11	Cycloheximide	0.467	69.78%	0.51	-0.042	-2.996	-0.162
BF06	(-) -Anisomycin	0.244	80.65%	0.574	0.134	-2.932	-0.301
BG06	Bortezomib	0.292	54.25%	0.235	-0.736	-4.102	-1.397
BG07	Pimozide	0.399	85.97%	0.137	0.071	-1.314	0.101

[a]**log Papp in 10^{-6} cm/s;** [b]**Volume of distribution (log L/kg) - low if below -0.1**5; high if above 0.45; [c]compounds with logPS > -2 are predicted to penetrate CNS, and with logPS < -3 unable to penetrate.; [d]compounds with logBB > 0.03 are considered to readily cross BBB and < -1 poorly permeable.

For BBB permeability, LogBB values above 0.3 predict that a compound could readily cross the BBB, and the ones with < -1 are poorly permeable [45]. According to this platform, none of the drugs and compounds selected from Covid-Box and most of the current ones used for toxoplasmosis treatment showed prediction for high crossing into the brain. However, thirteen (AA02, AA04, AE06, AG03, AG04, AG08, AH03, BA07, BA09, BB10, BD11, BF06, and BG07) showed values > -1. Of the drugs already used in the treatment of toxoplasmosis, the only one with a value above 0.3 was ATO (0.401 log BB). PYR presented a value close to the expected value (0.278 log BB) (Table 3).

Using the SwissADME platform, we obtained the Boilled-Egg graph, which also predicts if the drugs have the potential to cross the BBB and have high gastrointestinal absorption (HIA). The BBB permeability data provided by pkCSM was compared with the one provided in the Swiss ADME Boilled-Egg plot [42]. Of the analyzed drugs used for toxoplasmosis treatment, only PYR and ATO showed characteristics with potential BBB permeability at the points drawn above the egg yolk in the graph (yellow color) (Figure 2). The pkCSM program predicted that only ATO could cross the BBB (Table 3). On the same graph, it is possible to predict the compounds' passive gastrointestinal absorption (HIA) properties. Those that were plotted in the egg white region (SDZ and CLI) would be more easily absorbed in the gastrointestinal tract by passive transport than the compounds that were plotted in the gray region of the graph (AZT) (Figure 2A). In addition, the graph provides information such as whether the drugs are glycoprotein inhibitors. Only PYR, SDZ, and ATO drugs

 doi:10.20944/preprints202408.1034.v1

are not P-gp substrates (marked with red dots in the graph) (Figure 2A). Compounds that are P-gp inhibitors show increased absorption, while P-gp substrates reduce their absorption [46].

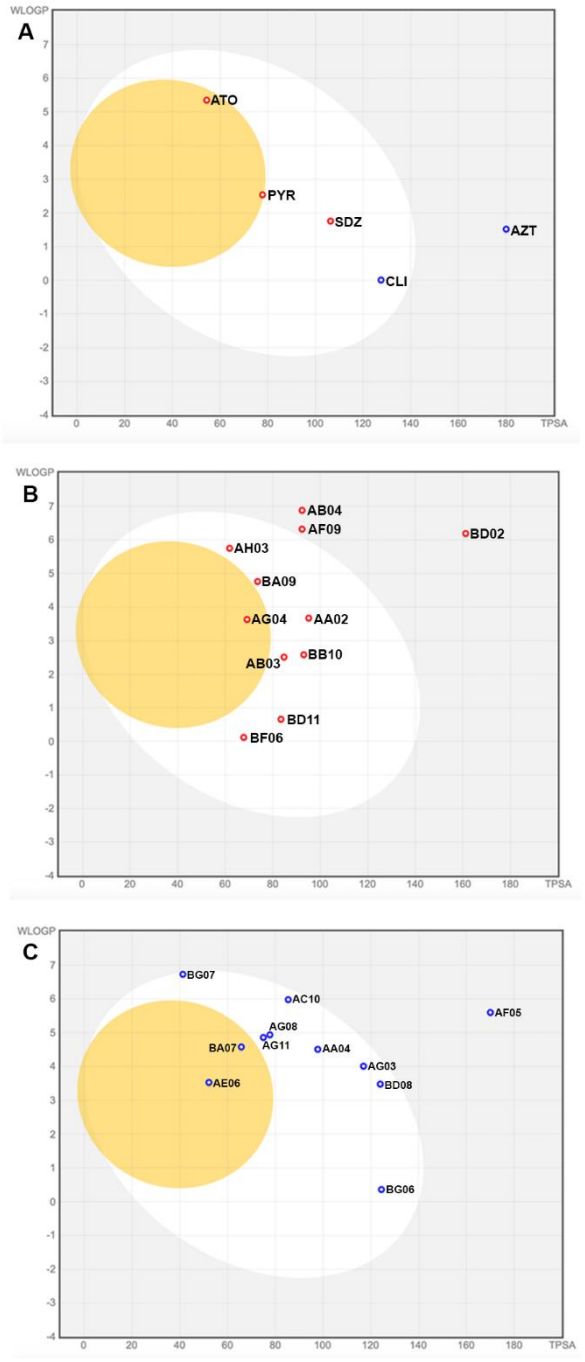

Figure 2. A-C. Boilled-Egg graph obtained through the SwissADME platform. Yellow part represents LogBB values = compounds that show highly probable blood-brain barrier (BBB) permeation; White part represents HIA values = highly probable gastrointestinal absorption; Red dots represent PGP- = non-P-gp substrate; Blue dots represent PGP+ = P-gp substrate. (A) PYR= Pyrimethamine; SDZ= Sulfadiazine; CLI= Clindamycin; AZT= Azithromycin; ATO= Atovaquone. (B) AA02= Niclosamide; AB03= Apilimod; AB04= Regonofarib; AF09= Sorafenib; AG04= Almitrine; AH03= Tetrandrine; BA09= Berbamine; BB10= Mycophenolic acid; BD02= Salinomycin; BD11= Cycloheximide; BF06= (-)-Anisomycin. (C) AA04= Bemcentinib; AC10= LY2228820; AD02= Digoxin (out of coverage area); AE06= Emetine; AF05= Ivermectin; AG03= Manidipine; AG08= Midostaurin; AG11= Abemaciclib; BA07= Ponatinib; BD08= Merimepodib; BG06= Bortezomib; BG07= Pimozide.

 doi:10.20944/preprints202408.1034.v1

Of Covid-Box, AG04 (Figure 2B), AE06, and BA07 (Figure 2C) presented characteristics with potential permeability to the BBB (points drawn in the upper part of the yolk of the graph) (Figure 2B-C); this information complies with the results obtained for BBB permeability with pKCSM. According to the results obtained in this analysis, none of the others are predictable for readily crossing the natural protections of the CNS [47]. The drugs AA02, AA04, AB03, AC10, AD02, AG03, AG08, AG11, AH03, BA09, BB10, BD08, BD11, BF06, BG06, and BG07 (Figure 2B-C) show potential for an easier absorption in the gastrointestinal tract by passive transport. Of the Covid-Box drugs: AA02, AB03, AB04, AF09, AG04, AH03, BA09, BB10, BD02, BD11, and BF06 are non-P-gp substrate (marked with red dots in graph) (Figure 2B) and AA04, AC10, AD02, AE06, AF05, AG03, AG11, BA07, BD08, BG06, and BG07 are P-gp substrates substrate (marked with blue dots in graph) (Figure 2C).

3.3. Analysis of the Effect on Ultrastructure Induced by Drugs and Compounds of Covid-Box by Transmission Electron Microscopy (TEM)

To confirm that selected Covid-Box drugs and compounds exert a direct effect on T. gondii, we analyzed the ultrastructure by TEM of tachyzoites after the treatment with Cycloheximide (BD11), Bortezomib (BG06), (-)-Anisomycin (BF06), Ivermectin (AF05), Almitrine (AG04), and Merimepodib (BD08) (Figures 3-5).

Untreated parasites showed normal morphology and organization (Figure 3A-B), tachyzoites treated with Cycloheximide at a concentration of 62.5 nM show increased endoplasmic reticulum area (stars) and alterations on the plasma membrane structure (arrowhead) (Figure 3C). When tachyzoites were treated with 125 nM Cycloheximide, it was observed that vacuoles containing parasites were completely lysed; the asterisk shows the disruption of the cell membrane (Figure 3D). Parasites treated with the drug Bortezomib at a concentration of 62.5 nM showed Golgi complex alteration (white arrow and star in Figure 3E), disruption of nucleus (N) division, as evidenced by the presence of two and three nucleus profiles in Figures 3E and 3F, respectively. Treatment with Bortezomib also caused vacuolization of tachyzoites cytoplasm (asterisks Figure 3F).

The tachyzoites treated with 100 nM (-)-Anisomycin (BF06) showed disorganization of the endoplasmic reticulum architecture (stars in Figure 4A-B, and inset B). It was also possible to observe drastic changes in the morphology and cell division of the parasite, making it possible to observe a single parasite with two nuclei (N) (Figure 4C). Treatment with 1µM Ivermectin (AF05) (Figure 4D-F) induced the formation of myelin-like structures [48,49] (arrowhead in Figure 4D and inset), resembling a process of cell death by autophagy. In Figures 4E-F, it is possible to observe tachyzoites showing intense vacuolization process (asterisks).

 doi:10.20944/preprints202408.1034.v1

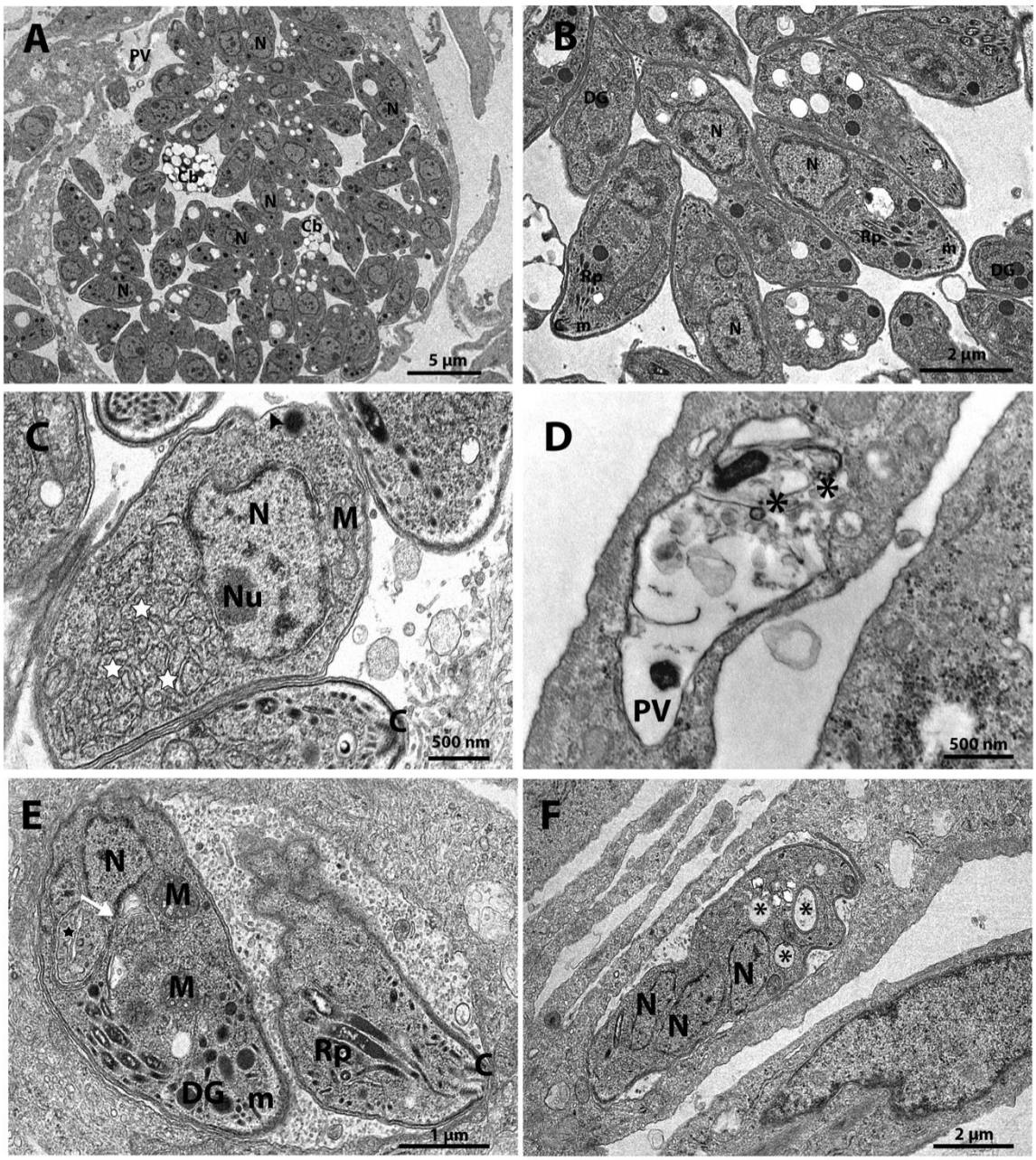

Figure 3. A-F. Transmission electron microscopy and analysis of the ultrastructure of the parasite *T. gondii* triggered by the compounds of the Covid-Box (BD11- Cycloheximide) and (BG06 - Bortezomib). The parasites were treated with the compounds for 48h. (A) The untreated parasites showed normal morphology; it is possible to observe a rosette of parasites inside the parasitophore vacuole. (B) Untreated parasites have a single mitochondrion, the apicoplast has four membranes, and the nucleolus can be seen in the nucleus. (C) Parasites treated with the drug 62.5 nM Cycloheximide showed an increase of the endoplasmic reticulum area (stars) and alterations in the structure of the plasmatic membrane; it is possible to observe only a simple membrane (black arrowhead). (D) Parasites treated with 125 nM BD11 were completely destroyed; it is possible to observe disruption of the cell membrane. (E) Parasites treated with 62.5 nM Bortezomib showed Golgi complex alteration (white arrow), and the Golgi complex was surrounded by the nuclear envelope (black star). (F) Parasites treated with 62.5 nM Bortezomib showed impairment of cell division with three nucleus profiles and intense cytoplasmic vacuolization (asterisks). A - Apicoplast; C - Conoid; Cb – Corpuscle basal; DG - Dense granules; M - Mitochondria; m – Micronemes; N - Nucleus; Rp – Rhoptries; Nu - Nucleolus; PV – Parasitophorous Vacuole.

 doi:10.20944/preprints202408.1034.v1

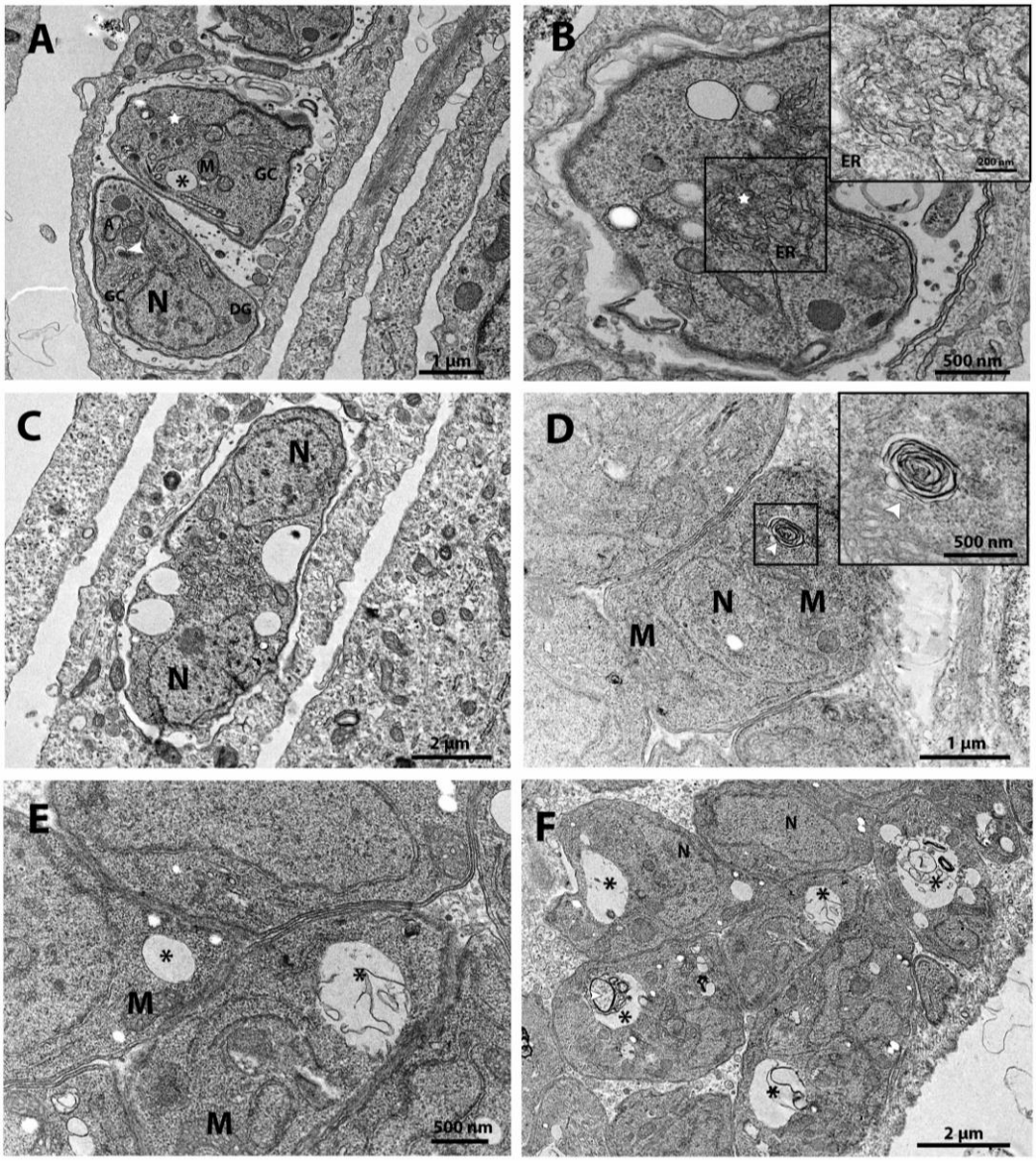

Figure 4. A-F. Transmission electron microscopy of the *T. gondii* treated BF06 - (-)-Anisomycin) and AF05 - Ivermectin. The parasites were treated with the drugs for 48 hours. (A) Parasites treated with 100 nM - (-)-Anisomycin showed an increase of the endoplasmic reticulum area (star). (B) 100 nM - (-)-Anisomycin induced changes in the parasite's endoplasmic reticulum (star in inset). (C) 100 nM - (-)-Anisomycin also induced impairment of the cell division, making it possible to observe a single parasite with two nuclei. (D) Parasites treated with 1 µM Ivermectin induced the formation of myelin-like figures (inset - white arrowhead). (E) Parasites treated with 1 µM Ivermectin showed vacuoles inside the parasite body (asterisks). (F) In this figure, it is also possible to observe the intense vacuolization process in parasites treated with 1µM Ivermectin (asterisks). A - Apicoplast; DG - Dense Granules; M - Mitochondria; N - Core; GC - Golgi complex; ER - Endoplasmic Reticulum.

Treatment of the tachyzoites with 1 µM Almitrine (AG04) also induced myelin-like structures (inset in Figure 5A) and impairment of the parasite's cell division (Figure 5B). Figure 5B shows a mass of mother cell in a drastic vacuolization process (asterisks) containing two daughter cells. Figure 5C and inset also show a tachyzoite presenting Golgi complex (GC) disorganization. Changes in the Golgi complex (GC in Figures 5D-E) were also observed in parasites treated with 1.5 µM Merimepodib (BD08). We also observed disorganization of the rhoptries (inset in Figure 5E) and an intense vacuolization process (asterisks in Figure 5F) after treatment with Merimepodib.

 doi:10.20944/preprints202408.1034.v1

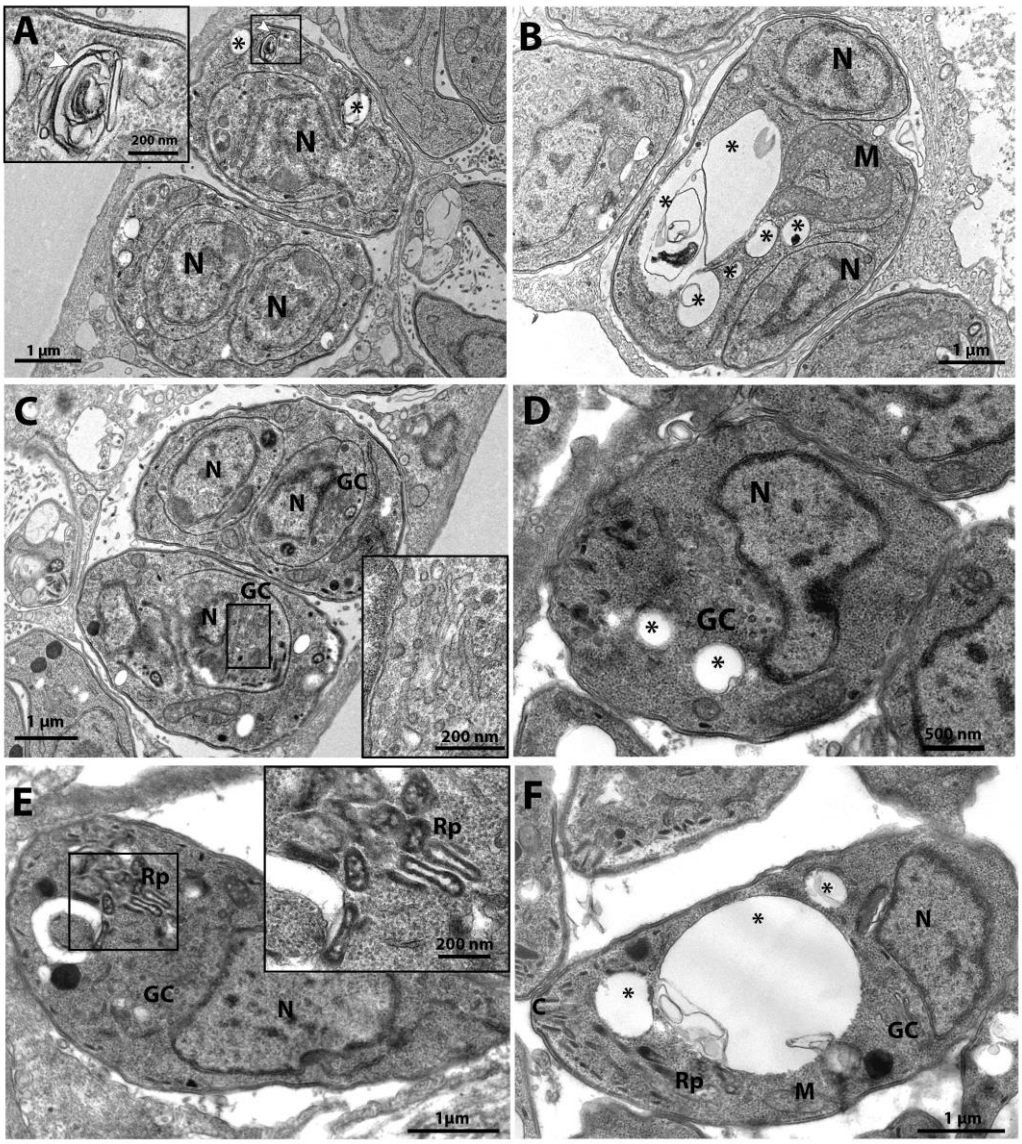

Figure 5. A-F. Transmission electron microscopy of the *T. gondii* after treatment with the drugs AG04 -Almitrine and BD08 – Merimepodib for 48h. (A) Parasites treated with almitrine at a concentration of 1 µM showed an alteration in the cell division process, and it was possible to see two daughter cells in a single parasite; it was also possible to observe a process suggestive of autophagy in the tachyzoites (detail - white arrowhead in insert). (B) After treatment with almitrine, we also observed an intense vacuolization process (asterisks). (C) In addition, 1 µM almitrine also induced fragmentation of the Golgi complex (insert). (D) Parasites treated with 1.5 µM merimepodib induced Golgi complex fragmentation. (E) Another important alteration observed after treatment with 1.5 µM merimepodib was rhoptry disorganization, which can be seen at a higher magnification in the insert. (F) In this figure, it is also possible to observe the intense process of vacuolization in parasites treated with 1.5 µM merimepodib (asterisks). M - Mitochondria; N - Nucleus; GC - Golgi complex; Rp - Rhoptries.

4. Discussion

In vitro tests were performed to evaluate the potential of applying the drugs and compounds present in the Covid-Box against *T. gondii* infection and to demonstrate the potential of the antiproliferative effect of the drugs and compounds in the Covid-Box. After these, we selected 23 drugs and compounds that could inhibit the proliferation of the parasite by more than 70%. The discovery of new uses of drugs previously used for other pharmaceutical purposes is a cheaper solution for treating neglected diseases. The antiproliferative analysis showed that the selected

 doi:10.20944/preprints202408.1034.v1

compounds inhibited *T. gondii* proliferation with values of IC_{50}s ranging from 0.02 μM and 0.74 μM, and ten showed IC_{50} lower than 100 nM (Table 1). Cytotoxicity analysis by the MTS assay also showed that most compounds were highly selective for *T. gondii* (Table 1). Of the 23 drugs, 11 were recently reported in a study of the anti-*T. gondii* effect of Covid box compounds, but three (Apilimode, Midostaurin, and Salinomycin) have been reported here for the first time. However, this is the first work to demonstrate the ultrastructural alterations caused by Cycloheximide, Bortezomib, (-)-Anisomycin, Ivermectin, Almitrine, and Merimepodib in tachyzoites through TEM analysis.

Our research identified Cycloheximide, (-)-Anisomycin, and Bortezomib as the most potent drugs against *T. gondii* tachyzoites, inhibiting parasite proliferation with IC_{50}s in the range of 20-30 nM. This finding is in line with the study by Fichera, Bhopale, and Ross (1995) [41], which found an IC_{50} value of 0.01 μM after 48 hours of treatment with (-)-Anisomycin, a value in the nanomolar range. In addition, *in silico* analyses demonstrated that Cycloheximide and (-)-Anisomycin show the predictors of good oral bioavailability according to Lipinski's rule of 5 (RO5) and Veber, while Bortezomib violates only one predictor (Table 2)[50]. *In silico* analysis also showed that Cycloheximide and (-)-Anisomycin are also non-P-gp substrates, have highly probable gastrointestinal absorption, and potential to cross the BBB (Tables 2, 3 and Figure 2)

Cycloheximide and (-)-Anisomycin are inhibitors of protein synthesis in other pathogens [51,52]. MET analyses showed an increase in the endoplasmic reticulum area of *T. gondii* after treatment with 62.5 nM cycloheximide (Asterisks in Fig. 3C) and 100 nM (-) Anisomycin (Fig. 4B-C). The endoplasmic reticulum also synthesizes essential lipids to maintain the plasma membrane [53,54]. Interestingly, similar ultrastructural changes were observed when *T. gondii* was treated with the antifungal drugs itraconazole, eberconazole, and thiolactomycin analogues [21,28]. The treatment *T. gondii* with this last affected the acylglycerol synthesis by the endoplasmic reticulum [55].

The drug Bortezomib is a proteasome inhibitor. Proteasomes are responsible for the degradation of defective proteins in the cell and are considered a crucial point in the stability of regulatory proteins. Proteasome inhibitors are known to cause cell death [56,57]. Other authors have reported the inhibition of catalytic subunits of the proteasome in Plasmodium falciparum [58,59]. This finding is in line with our data since we observed the formation of structures suggestive of an autophagic process in parasites treated with 62.5 nM Bortezomib by TEM. Adeyemi et al., (2019) [33] found an IC_{50} value of 0.101μM for Bortezomib against *T. gondii* tachyzoites after 72 hours of treatment. Cajazeiro et al., (2022) [23] found a different EC_{50} value of 0.22 μM after 72 hours of treatment, which differs slightly from the IC_{50} value found in this study after treatment with Bortezomib (0.03 μM). This difference is possible due to the longer treatment time used by us in this study, which suggests a time dependent effect of this drug. Therefore, the sum of the results obtained here supports that Cycloheximide, (-)-Anisomycin, and Bortezomib can be potential drugs for treating the acute phase of toxoplasmosis.

In our study, Ivermectin was another drug with anti-*T. gondii* activity. The potential activity of Ivermectin against *T. gondii* and other protozoa, such as *Giardia lamblia*, *Trypanosoma cruzi*, *Leishmania infantum*, and *Trypanosoma evansi*, has also been reported in the literature [36,60–63]. However, this is the first study showing the ultrastructural alterations in a parasite from the Apicomplexa phylum. Using TEM, we observed that the treatment with 1 μM Ivermectin for 48 hours induced an intense process of vacuolation and changes in the *T. gondii*'s cell division, confirming a direct effect against this parasite and suggesting death by autophagic induction. A similar effect was observed after the treatment of glioma cells with Ivermectin [64]. Treatment of *T. gondii* tachyzoites with Almitrine also caused an intense vacuolization and formation of myelin-like structures (Figure 4A-D), also suggestive of autophagic process induction. Almitrine is already used in clinics to treat diseases that affect the respiratory system. It's in vitro and in vivo effects against *T. gondii* have been recently reported [23,24] with IC_{50} values of 0.42 μM and 0.32 μM after 72 hours of treatment, respectively, which are close to the that found in this study.

Mycophenolic acid and Merimepodib are antiviral inhibitors of IMP-dehydrogenase, affecting DNA and RNA synthesis [65]. These drugs affected *T. gondii* proliferation with IC_{50} of 0.07 μM and 0.48 μM, respectively. Previous studies showed IC_{50}s of 211 μM (mycophenolic acid) and 0.78 μM

 doi:10.20944/preprints202408.1034.v1

(merimepodib) for *T. gondii* tachyzoites after 24 and 72 h of treatment, respectively [24]. Merimepodib also showed a high selective index for *T. gondii* compared with HFF cells (human foreskin fibroblasts) [24]. Analyses by TEM showed that merimepodib caused *T. gondii* Golgi complex fragmentation, rhoptry disorganization, and intense vacuolation (Figure 4D-F). These results suggest that this drug could affect *T. gondii*, interfering with its secretory pathway.

Developing a new infectious disease treatment is complex because medicines must be absorbed, reach adequate plasma concentrations, and be distributed to tissues and cellular compartments where the infection is present in the body. In the case of toxoplasmosis, this is even more critical, as one of the main sites of infection is the CNS. Based on anti-*T. gondii* activity assay and to Lipinski's and Veber's predictor's analysis, the 23 drugs and compounds identified in this work are good candidates to become oral drugs since they inhibit *T. gondii* proliferation at submicromolar range and comply with RO5, showing no more than one violation. We can highlight that in addition to the compounds Cycloheximide, Bortezomib, Anisomycin, Almitrine, and Merimepodib analyzed by TEM, the drug Mycophenolic Acid also presented a micromolar IC_{50} range lower than 0.10 μM and did not violate Lipinski's rules and the predictors of Veber. In addition, these drugs also demonstrated desirable predictors for oral absorption (Table 2). However, we should not disregard the potential of drugs that did not comply with RO5 or presented values lower than expected for oral absorption or BBB permeability since AZT, a drug already commercialized, presented a value lower than expected (-0.211 log Papp at 10-6 cm/s) and intestinal Absorption (Human) = 45.808%), but despite AZT not having good intestinal absorption, this drug is used to treat toxoplasmosis [9].

5. Conclusions

After Covid-Box screening, we identified three new drugs with anti-*T. gondii* activity, making this is first study to report their effectiveness against this parasite. In total, 23 drugs were found to be promising candidates for further pre-clinical studies on toxoplasmosis. The discovery of these new drug candidates for the treatment of toxoplasmosis is of great relevance and should be further explored for in vivo analysis in the future. The results presented here have shown that drug repurposing is a potential alternative for the treatment of infectious and neglected diseases and that the boxes provided by MMV are extremely important for solving the problems involved in treating these diseases.

Author Contributions: ESMD designed the project; ALOC, MS, RENL, RCV, and ESMD performed experiments; ALOC, MS, and ESMD analysed the results; ALOC, MS and ESMD wrote the manuscript; RCV revised the manuscript; RCV and ESMD develop with reagents and materials. All authors reviewed the manuscript.

Funding: This work was supported by the Coordenação de Aperfeiçoamento de Pessoal de Nível Superior (CAPES), Conselho Nacional de Desenvolvimento Científico e Tecnológico (CNPq), and Pró-Reitoria de Pesquisa-Universidade Federal de Minas Gerais.

Data Availability Statement: The original contributions presented in this study are included in the paper. Further inquiries can be directed to the corresponding author.

Acknowledgments: MMV for supplying the Covid-Box. TEM analyses were carried out in the Center of Microscopy at the Universidade Federal de Minas Gerais, Belo Horizonte and and in the Centro Nacional de Biologia Estrutural e Bioimagem, Rio de Janeiro, Brazil.

Conflicts of Interest: The authors declare no conflict of interest.

References

1. Bigna, J.J.; Tochie, J.N.; Tounouga, D.N.; Bekolo, A.O.; Ymele, N.S.; Youda, E.L.; Sime, P.S.; Nansseu, J.R. Global, Regional, and Country Seroprevalence of *Toxoplasma gondii* in Pregnant Women: A Systematic Review, Modelling and Meta-Analysis. *Sci Rep* **2020**, *10*, 12102, doi:10.1038/s41598-020-69078-9.
2. Robert-Gangneux, F.; Dardé, M.-L. Epidemiology of and Diagnostic Strategies for Toxoplasmosis. *Clin Microbiol Rev* **2012**, *25*, 264–296, doi:10.1128/CMR.05013-11.
3. Zangerle, R.; Allerberger, F.; Pohl, P.; Fritsch, P.; Dierich, M.P. High Risk of Developing Toxoplasmic Encephalitis in AIDS Patients Seropositive to Toxoplasma Gondii. *Med Microbiol Immunol* **1991**, *180*, doi:10.1007/BF00193846.

4. Vasconcelos-Santos, D.V.; Machado Azevedo, D.O.; Campos, W.R.; Oréfice, F.; Queiroz-Andrade, G.M.; Carellos, É.V.M.; Castro Romanelli, R.M.; Januário, J.N.; Resende, L.M.; Martins-Filho, O.A. Congenital Toxoplasmosis in Southeastern Brazil: Results of Early Ophthalmologic Examination of a Large Cohort of Neonates. *Ophthalmology* **2009**, *116*, 2199-2205.e1, doi:10.1016/j.ophtha.2009.04.042.
5. Gilbert, R.E. Is Ocular Toxoplasmosis Caused by Prenatal or Postnatal Infection? *British Journal of Ophthalmology* **2000**, *84*, 224–226, doi:10.1136/bjo.84.2.224.
6. Gilbert, R.E.; Freeman, K.; Lago, E.G.; Bahia-Oliveira, L.M.G.; Tan, H.K.; Wallon, M.; Buffolano, W.; Stanford, M.R.; Petersen, E.; for The European Multicentre Study on Congenital Toxoplasmosis (EMSCOT) Ocular Sequelae of Congenital Toxoplasmosis in Brazil Compared with Europe. *PLoS Negl Trop Dis* **2008**, *2*, e277, doi:10.1371/journal.pntd.0000277.
7. Jones, J.L.; Lopez, A.; Wilson, M.; Schulkin, J.; Gibbs, R. Congenital Toxoplasmosis: A Review. *Obstetrical and Gynecological Survey*.
8. Diesel, A.A.; Zachia, S.D.A.; Müller, A.L.L.; Perez, A.V.; Uberti, F.A.D.F.; Magalhães, J.A.D.A. Follow-up of Toxoplasmosis during Pregnancy: Ten-Year Experience in a University Hospital in Southern Brazil. *Rev Bras Ginecol Obstet* **2019**, *41*, 539–547, doi:10.1055/s-0039-1697034.
9. Dunay, I.R.; Gajurel, K.; Dhakal, R.; Liesenfeld, O.; Montoya, J.G. Treatment of Toxoplasmosis: Historical Perspective, Animal Models, and Current Clinical Practice. *Clin Microbiol Rev* **2018**, *31*, e00057-17, doi:10.1128/CMR.00057-17.
10. Neville, A.J.; Zach, S.J.; Wang, X.; Larson, J.J.; Judge, A.K.; Davis, L.A.; Vennerstrom, J.L.; Davis, P.H. Clinically Available Medicines Demonstrating Anti-*Toxoplasma* Activity. *Antimicrob Agents Chemother* **2015**, *59*, 7161–7169, doi:10.1128/AAC.02009-15.
11. Silva, L.A.; Reis-Cunha, J.L.; Bartholomeu, D.C.; Vítor, R.W.A. Genetic Polymorphisms and Phenotypic Profiles of Sulfadiazine-Resistant and Sensitive *Toxoplasma gondii* Isolates Obtained from Newborns with Congenital Toxoplasmosis in Minas Gerais, Brazil. *PLoS ONE* **2017**, *12*, e0170689, doi:10.1371/journal.pone.0170689.
12. Silva, L.A.; Fernandes, M.D.; Machado, A.S.; Reis-Cunha, J.L.; Bartholomeu, D.C.; Almeida Vitor, R.W. Efficacy of Sulfadiazine and Pyrimetamine for Treatment of Experimental Toxoplasmosis with Strains Obtained from Human Cases of Congenital Disease in Brazil. *Experimental Parasitology* **2019**, *202*, 7–14, doi:10.1016/j.exppara.2019.05.001.
13. De Lima Bessa, G.; Vitor, R.W.D.A.; Lobo, L.M.S.; Rêgo, W.M.F.; De Souza, G.C.A.; Lopes, R.E.N.; Costa, J.G.L.; Martins-Duarte, E.S. In Vitro and in Vivo Susceptibility to Sulfadiazine and Pyrimethamine of *Toxoplasma gondii* Strains Isolated from Brazilian Free Wild Birds. *Sci Rep* **2023**, *13*, 7359, doi:10.1038/s41598-023-34502-3.
14. Xue, H.; Li, J.; Xie, H.; Wang, Y. Review of Drug Repositioning Approaches and Resources. *Int. J. Biol. Sci.* **2018**, *14*, 1232–1244, doi:10.7150/ijbs.24612.
15. Jourdan, J.-P.; Bureau, R.; Rochais, C.; Dallemagne, P. Drug Repositioning: A Brief Overview. *Journal of Pharmacy and Pharmacology* **2020**, *72*, 1145–1151, doi:10.1111/jphp.13273.
16. Boyom, F.F.; Fokou, P.V.T.; Tchokouaha, L.R.Y.; Spangenberg, T.; Mfopa, A.N.; Kouipou, R.M.T.; Mbouna, C.J.; Donfack, V.F.D.; Zollo, P.H.A. Repurposing the Open Access Malaria Box To Discover Potent Inhibitors of *Toxoplasma gondii* and Entamoeba Histolytica. *Antimicrob Agents Chemother* **2014**, *58*, 5848–5854, doi:10.1128/AAC.02541-14.
17. Subramanian, G.; Belekar, M.A.; Shukla, A.; Tong, J.X.; Sinha, A.; Chu, T.T.T.; Kulkarni, A.S.; Preiser, P.R.; Reddy, D.S.; Tan, K.S.W.; et al. Targeted Phenotypic Screening in Plasmodium Falciparum and *Toxoplasma gondii* Reveals Novel Modes of Action of Medicines for Malaria Venture Malaria Box Molecules. *mSphere* **2018**, *3*, e00534-17, doi:10.1128/mSphere.00534-17.
18. Varberg, J.M.; LaFavers, K.A.; Arrizabalaga, G.; Sullivan, W.J. Characterization of Plasmodium Atg3-Atg8 Interaction Inhibitors Identifies Novel Alternative Mechanisms of Action in *Toxoplasma gondii*. *Antimicrob Agents Chemother* **2018**, *62*, e01489-17, doi:10.1128/AAC.01489-17.
19. Spalenka, J.; Escotte-Binet, S.; Bakiri, A.; Hubert, J.; Renault, J.-H.; Velard, F.; Duchateau, S.; Aubert, D.; Huguenin, A.; Villena, I. Discovery of New Inhibitors of *Toxoplasma gondii* via the Pathogen Box. *Antimicrob Agents Chemother* **2018**, *62*, e01640-17, doi:10.1128/AAC.01640-17.
20. Radke, J.B.; Burrows, J.N.; Goldberg, D.E.; Sibley, L.D. Evaluation of Current and Emerging Antimalarial Medicines for Inhibition of *Toxoplasma gondii* Growth in Vitro. *ACS Infect. Dis.* **2018**, *4*, 1264–1274, doi:10.1021/acsinfecdis.8b00113.
21. dos Santos, M.; Oliveira Costa, A.L.; Vaz, G.H. de S.; de Souza, G.C.A.; Vitor, R.W. de A.; Martins-Duarte, É.S. Medicines for Malaria Venture Pandemic Box In Vitro Screening Identifies Compounds Highly Active against the Tachyzoite Stage of *Toxoplasma gondii*. *Tropical Medicine and Infectious Disease* **2023**, *8*, doi:10.3390/tropicalmed8120510.
22. Dos Santos, B.R.; Ramos, A.B.D.S.B.; De Menezes, R.P.B.; Scotti, M.T.; Colombo, F.A.; Marques, M.J.; Reimão, J.Q. Anti- *Toxoplasma gondii* Screening of MMV Pandemic Response Box and Evaluation of RWJ-

67657 Efficacy in Chronically Infected Mice. *Parasitology* **2023**, *150*, 1226–1235, doi:10.1017/S0031182023000999.

23. Cajazeiro, D.C.; Toledo, P.P.M.; De Sousa, N.F.; Scotti, M.T.; Reimão, J.Q. Drug Repurposing Based on Protozoan Proteome: In Vitro Evaluation of In Silico Screened Compounds against *Toxoplasma gondii*. *Pharmaceutics* **2022**, *14*, 1634, doi:10.3390/pharmaceutics14081634.
24. Dos Santos, B.R.; Ramos, A.B.D.S.B.; De Menezes, R.P.B.; Scotti, M.T.; Colombo, F.A.; Marques, M.J.; Reimão, J.Q. Repurposing the Medicines for Malaria Venture's COVID Box to Discover Potent Inhibitors of *Toxoplasma gondii*, and in Vivo Efficacy Evaluation of Almitrine Bismesylate (MMV1804175) in Chronically Infected Mice. *PLoS ONE* **2023**, *18*, e0288335, doi:10.1371/journal.pone.0288335.
25. Barltrop, J.A.; Owen, T.C.; Cory, A.H.; Cory, J.G. 5-(3-Carboxymethoxyphenyl)-2-(4,5-Dimethylthiazolyl)-3-(4-Sulfophenyl)Tetrazolium, Inner Salt (MTS) and Related Analogs of 3-(4,5-Dimethylthiazolyl)-2,5-Diphenyltetrazolium Bromide (MTT) Reducing to Purple Water-Soluble Formazans As Cell-Viability Indicators. *Bioorganic & Medicinal Chemistry Letters* **1991**, *1*, 611–614, doi:10.1016/S0960-894X(01)81162-8.
26. Martins-Duarte, E.S.; Portes, J. de A.; da Silva, R.B.; Pires, H.S.; Garden, S.J.; de Souza, W. In Vitro Activity of N-Phenyl-1,10-Phenanthroline-2-Amines against Tachyzoites and Bradyzoites of *Toxoplasma gondii*. *Bioorganic & Medicinal Chemistry* **2021**, *50*, 116467, doi:10.1016/j.bmc.2021.116467.
27. Martins-Duarte, E.S.; Dubar, F.; Lawton, P.; França Da Silva, C.; C. Soeiro, M.D.N.; De Souza, W.; Biot, C.; Vommaro, R.C. Ciprofloxacin Derivatives Affect Parasite Cell Division and Increase the Survival of Mice Infected with *Toxoplasma gondii*. *PLoS ONE* **2015**, *10*, e0125705, doi:10.1371/journal.pone.0125705.
28. Martins-Duarte, É.D.S.; De Souza, W.; Vommaro, R.C. Itraconazole Affects *Toxoplasma gondii* Endodyogeny:. *FEMS Microbiology Letters* **2008**, *282*, 290–298, doi:10.1111/j.1574-6968.2008.01130.x.
29. Martins-Duarte, É.S.; Lemgruber, L.; De Souza, W.; Vommaro, R.C. Toxoplasma Gondii: Fluconazole and Itraconazole Activity against Toxoplasmosis in a Murine Model. *Experimental Parasitology* **2010**, *124*, 466–469, doi:10.1016/j.exppara.2009.12.011.
30. Chang, H.R.; Comte, R.; Pechère, J.C. In Vitro and in Vivo Effects of Doxycycline on *Toxoplasma gondii*. *Antimicrob Agents Chemother* **1990**, *34*, 775–780, doi:10.1128/AAC.34.5.775.
31. McCabe, R.E.; Luft, B.J.; Remington, J.S. THE EFFECTS OF VYCLOSPORINE ON *TOXOPLASMA GONDII* IN VIVO AN IN VITRO: *Transplantation* **1986**, *41*, 611–615, doi:10.1097/00007890-198605000-00012.
32. Dittmar, A.J.; Drozda, A.A.; Blader, I.J. Drug Repurposing Screening Identifies Novel Compounds That Effectively Inhibit *Toxoplasma gondii* Growth. *mSphere* **2016**, *1*, e00042-15, doi:10.1128/mSphere.00042-15.
33. Adeyemi, O.S.; Atolani, O.; Awakan, O.J.; Olaolu, D.; Nwonuma, C.O.; Alejolowo, O.; Otohinoyi, D.A.; Rotimi, D.; Owolabi, A.; Batiha, G.E.-S. In Vitro Screening to Identify Anti-*Toxoplasma* Compounds and In Silico Modeling for Bioactivities and Toxicity. **2019**.
34. Zhang, J.L.; Si, H.F.; Shang, X.F.; Zhang, X.K.; Li, B.; Zhou, X.Z.; Zhang, J.Y. New Life for an Old Drug: In Vitro and in Vivo Effects of the Anthelmintic Drug Niclosamide against *Toxoplasma gondii* RH Strain. *International Journal for Parasitology: Drugs and Drug Resistance* **2019**, *9*, 27–34, doi:10.1016/j.ijpddr.2018.12.004.
35. Gurnett, A.M.; Dulski, P.M.; Darkin-Rattray, S.J.; Carrington, M.J.; Schmatz, D.M. Selective Labeling of Intracellular Parasite Proteins by Using Ricin. *Proc. Natl. Acad. Sci. U.S.A.* **1995**, *92*, 2388–2392, doi:10.1073/pnas.92.6.2388.
36. Bilgin, M.; Yildirim, T.; Hokelek, M. In Vitro Effects ofIvermectin and Sulphadiazine on *Toxoplasma gondii*. *Balkan Med J* **2013**, *30*, 19–22, doi:10.5152/balkanmedj.2012.098.
37. Shang, F.-F.; Wang, M.-Y.; Ai, J.-P.; Shen, Q.-K.; Guo, H.-Y.; Jin, C.-M.; Chen, F.-E.; Quan, Z.-S.; Jin, L.; Zhang, C. Synthesis and Evaluation of Mycophenolic Acid Derivatives as Potential Anti-*Toxoplasma gondii* Agents. *Med Chem Res* **2021**, *30*, 2228–2239, doi:10.1007/s00044-021-02803-9.
38. Castro-Elizalde, K.N.; Hernández-Contreras, P.; Ramírez-Flores, C.J.; González-Pozos, S.; Gómez De León, C.T.; Mondragón-Castelán, M.; Mondragón-Flores, R. Mycophenolic Acid Induces Differentiation of *Toxoplasma gondii* RH Strain Tachyzoites into Bradyzoites and Formation of Cyst-like Structure in Vitro. *Parasitol Res* **2018**, *117*, 547–563, doi:10.1007/s00436-017-5738-x.
39. Egawa, Y.; Oshima, S.; Umezawa, S. Studies on Cycloheximide-Related Compounds. I Esters of Cycloheximide and Their Antitoxoplasmic Activity 1965.
40. Beckers, C.J.; Roos, D.S.; Donald, R.G.; Luft, B.J.; Schwab, J.C.; Cao, Y.; Joiner, K.A. Inhibition of Cytoplasmic and Organellar Protein Synthesis in *Toxoplasma gondii*. Implications for the Target of Macrolide Antibiotics. *J. Clin. Invest.* **1995**, *95*, 367–376, doi:10.1172/JCI117665.
41. Fichera, M.E.; Bhopale, M.K.; Roos, D.S. In Vitro Assays Elucidate Peculiar Kinetics of Clindamycin Action against *Toxoplasma gondii*. *Antimicrob Agents Chemother* **1995**, *39*, 1530–1537, doi:10.1128/AAC.39.7.1530.
42. Daina, A.; Michielin, O.; Zoete, V. SwissADME: A Free Web Tool to Evaluate Pharmacokinetics, Drug-Likeness and Medicinal Chemistry Friendliness of Small Molecules. *Sci Rep* **2017**, *7*, 42717, doi:10.1038/srep42717.

43. Lipinski, C.A.; Lombardo, F.; Dominy, B.W.; Feeney, P.J. Experimental and Computational Approaches to Estimate Solubility and Permeability in Drug Discovery and Development Settings. *Advanced Drug Delivery Reviews* **1997**, *23*, 3–25, doi:10.1016/S0169-409X(96)00423-1.
44. Veber, D.F.; Johnson, S.R.; Cheng, H.-Y.; Smith, B.R.; Ward, K.W.; Kopple, K.D. Molecular Properties That Influence the Oral Bioavailability of Drug Candidates. *J. Med. Chem.* **2002**, *45*, 2615–2623, doi:10.1021/jm020017n.
45. Pires, D.E.V.; Blundell, T.L.; Ascher, D.B. pkCSM: Predicting Small-Molecule Pharmacokinetic and Toxicity Properties Using Graph-Based Signatures. *J. Med. Chem.* **2015**, *58*, 4066–4072, doi:10.1021/acs.jmedchem.5b00104.
46. Lynch, T.; Price, A. The Effect of Cytochrome P450 Metabolism on Drug Response, Interactions, and Adverse Effects. *Cytochrome P* **2007**, *76*.
47. Sanchez-Covarrubias, L.; Slosky, L.; Thompson, B.; Davis, T.; Ronaldson, P. Transporters at CNS Barrier Sites: Obstacles or Opportunities for Drug Delivery? *CPD* **2014**, *20*, 1422–1449, doi:10.2174/13816128113199990463.
48. Abdrakhmanov, A.; Gogvadze, V.; Zhivotovsky, B. To Eat or to Die: Deciphering Selective Forms of Autophagy. *Trends in Biochemical Sciences* **2020**, *45*, 347–364, doi:10.1016/j.tibs.2019.11.006.
49. Pedra-Rezende, Y.; Macedo, I.S.; Midlej, V.; Mariante, R.M.; Menna-Barreto, R.F.S. Different Drugs, Same End: Ultrastructural Hallmarks of Autophagy in Pathogenic Protozoa. *Front. Microbiol.* **2022**, *13*, 856686, doi:10.3389/fmicb.2022.856686.
50. Pichler, H.; Gaigg, B.; Hrastnik, C.; Achleitner, G.; Kohlwein, S.D.; Zellnig, G.; Perktold, A.; Daum, G. A Subfraction of the Yeast Endoplasmic Reticulum Associates with the Plasma Membrane and Has a High Capacity to Synthesize Lipids. *European Journal of Biochemistry* **2001**, *268*, 2351–2361, doi:10.1046/j.1432-1327.2001.02116.x.
51. Osborn, C.D.; Holloway, F.A. Can Commonly Used Antibiotics Disrupt Formation of New Memories? *Bull. Psychon. Soc.* **1984**, *22*, 356–358, doi:10.3758/BF03333842.
52. Macias-Silva, M.; Vazquez-Victorio, G.; Hernandez-Damian, J. Anisomycin Is a Multifunctional Drug: More than Just a Tool to Inhibit Protein Synthesis. *curr chem biol* **2010**, *4*, 124–132, doi:10.2174/187231310791170793.
53. Ramakrishnan, S.; Serricchio, M.; Striepen, B.; Bütikofer, P. Lipid Synthesis in Protozoan Parasites: A Comparison between Kinetoplastids and Apicomplexans. *Progress in Lipid Research* **2013**, *52*, 488–512, doi:10.1016/j.plipres.2013.06.003.
54. Martins-Duarte, É.S.; Carias, M.; Vommaro, R.; Surolia, N.; De Souza, W. Apicoplast Fatty Acid Synthesis Is Essential for Pellicle Formation at the End of Cytokinesis in *Toxoplasma gondii*. *Journal of Cell Science* **2016**, *129*, 3320–3331, doi:10.1242/jcs.185223.
55. Martins-Duarte, E.S.; Jones, S.M.; Gilbert, I.H.; Atella, G.C.; De Souza, W.; Vommaro, R.C. Thiolactomycin Analogues as Potential Anti-*Toxoplasma gondii* Agents. *Parasitology International* **2009**, *58*, 411–415, doi:10.1016/j.parint.2009.08.004.
56. Kisselev, A.F.; Callard, A.; Goldberg, A.L. Importance of the Different Proteolytic Sites of the Proteasome and the Efficacy of Inhibitors Varies with the Protein Substrate. *Journal of Biological Chemistry* **2006**, *281*, 8582–8590, doi:10.1074/jbc.M509043200.
57. Groll, M.; Huber, R.; Moroder, L. The Persisting Challenge of Selective and Specific Proteasome Inhibition. *Journal of Peptide Science* **2009**, *15*, 58–66, doi:10.1002/psc.1107.
58. Sridhar, S.; Bhat, G.; Guruprasad, K. Analysis of Bortezomib Inhibitor Docked within the Catalytic Subunits of the *Plasmodium falciparum* 20S Proteasome. *SpringerPlus* **2013**, *2*, 566, doi:10.1186/2193-1801-2-566.
59. Kreidenweiss, A.; Kremsner, P.G.; Mordmüller, B. Comprehensive Study of Proteasome Inhibitors against *Plasmodium falciparum* Laboratory Strains and Field Isolates from Gabon. *Malar J* **2008**, *7*, 187, doi:10.1186/1475-2875-7-187.
60. Mayol, G.F.; Revuelta, M.V.; Salusso, A.; Touz, M.C.; Rópolo, A.S. Evidence of Nuclear Transport Mechanisms in the Protozoan Parasite *Giardia lamblia*. *Biochimica et Biophysica Acta (BBA) - Molecular Cell Research* **2020**, *1867*, 118566, doi:10.1016/j.bbamcr.2019.118566.
61. Gupta, S.; Vohra, S.; Sethi, K.; Gupta, S.; Bera, B.C.; Kumar, S.; Kumar, R. In Vitro Anti-Trypanosomal Effect of Ivermectin on *Trypanosoma evansi* by Targeting Multiple Metabolic Pathways. *Trop Anim Health Prod* **2022**, *54*, 240, doi:10.1007/s11250-022-03228-1.
62. Fraccaroli, L.; Ruiz, M.D.; Perdomo, V.G.; Clausi, A.N.; Balcazar, D.E.; Larocca, L.; Carrillo, C. Broadening the Spectrum of Ivermectin: Its Effect on *Trypanosoma cruzi* and Related Trypanosomatids. *Front. Cell. Infect. Microbiol.* **2022**, *12*, 885268, doi:10.3389/fcimb.2022.885268.
63. Reis, T.A.R.; Oliveira-da-Silva, J.A.; Tavares, G.S.V.; Mendonça, D.V.C.; Freitas, C.S.; Costa, R.R.; Lage, D.P.; Martins, V.T.; Machado, A.S.; Ramos, F.F.; et al. Ivermectin Presents Effective and Selective Antileishmanial Activity in Vitro and in Vivo against *Leishmania infantum* and Is Therapeutic against Visceral Leishmaniasis. *Experimental Parasitology* **2021**, *221*, 108059, doi:10.1016/j.exppara.2020.108059.

 doi:10.20944/preprints202408.1034.v1

64. Liu, J.; Liang, H.; Chen, C.; Wang, X.; Qu, F.; Wang, H.; Yang, K.; Wang, Q.; Zhao, N.; Meng, J.; et al. Ivermectin Induces Autophagy-Mediated Cell Death through the AKT/mTOR Signaling Pathway in Glioma Cells. *Bioscience Reports* **2019**, *39*, BSR20192489, doi:10.1042/BSR20192489.
65. Sintchak, M.D.; Nimmesgern, E. The Structure of Inosine 5′-Monophosphate Dehydrogenase and the Design of Novel Inhibitors. *Immunopharmacology* **2000**, *47*, 163–184, doi:10.1016/S0162-3109(00)00193-4.